ORIGINAL ARTICLE

WILEY gebiology

Identification, distribution, and quantification of biominerals in a deciduous forest

C. Krieger[1] | C. Calvaruso[1] | C. Morlot[2,3] | S. Uroz[1,4,5] | L. Salsi[2,3] | M.-P. Turpault[1]

[1]INRA - UR 1138, Biogéochimie des Ecosystèmes Forestiers, Centre INRA de Nancy, Champenoux, France

[2]GéoRessources, UMR7359, Faculté des Sciences, Université de Lorraine, Vandœuvre-lès-Nancy, France

[3]GéoRessources, UMR7359, Faculté des Sciences, CNRS, Vandœuvre-lès-Nancy, France

[4]INRA - UMR1136, Interactions Arbres – Microorganismes, Centre INRA de Nancy, Champenoux, France

[5]Interactions Arbres – Microorganismes, UMR1136, Université de Lorraine, Vandœuvre-lès-Nancy, France

Correspondence
M.-P. Turpault, INRA – UR 1138, Biogéochimie des Ecosystèmes Forestiers, Centre INRA de Nancy, Champenoux, France.
Email: turpault@nancy.inra.fr

Present address
C. Calvaruso, EcoSustain, Environmental Engineering Office, Research and Development, Kanfen, France

Abstract

Biomineralization is a common process in most vascular plants, but poorly investigated for trees. Although the presence of calcium oxalate and silica accumulation has been reported for some tree species, the chemical composition, abundance, and quantification of biominerals remain poorly documented. However, biominerals may play important physiological and structural roles in trees, especially in forest ecosystems, which are characterized by nutrient-poor soils. In this context, our study aimed at investigating the morphology, distribution, and relative abundance of biominerals in the different vegetative compartments (foliage, branch, trunk, and root) of *Fagus sylvatica* L. and *Acer pseudoplatanus* L. using a combination of scanning electron microscopy and tomography analyses. Biomineral crystallochemistry was assessed by X-ray diffraction and energy-dispersive X-ray analyses, while calcium, silicon, and oxalic acid were quantified in the compartments and at the forest scale. Our analyses revealed that biominerals occurred as crystals or coating layers mostly in bark and leaves and were identified as opal, whewellite, and complex biominerals. In both tree species, opal was mostly found in the external tissues of trunk, branch, and leaves, but also in the roots of beech. In the stand, opal represents around 170 kg/ha. Whewellite was found to suit to conductive tissues (i.e., axial phloem parenchyma, vascular bundles, vessel element) in all investigated compartments of the two tree species. The shape of whewellite was prismatic and druses in beech, and almost all described shapes were seen in sycamore maple. Notably, the amount of whewellite was strongly correlated with the total calcium in all investigated compartments whatever the tree species is, suggesting a biologic control of whewellite precipitation. The amount of whewellite in the aboveground biomass of Montiers forest was more important than that of opal and was around 1170 kg/ha. Therefore, biominerals contribute in a substantial way to the biogeochemical cycles of silicon and calcium.

1 | INTRODUCTION

Biomineralization is a widespread process across the plant kingdom. Several physiological and ecological functions have been proposed for plants biominerals, such as an involvement in the bulk calcium regulation, in the detoxification of aluminum, oxalic acid, and heavy metals, in the regulation of ion balance, in the reduction of hydric, salt, and temperature stresses (Brown, Warwick, & Prychid, 2013; Currie & Perry, 2007; Franceschi & Nakata, 2005; He, Veneklaas, Kuo, & Lambers, 2014; Nakata, 2012; Sarret et al., 2006). They also contribute to the optimization of photosynthesis by gathering and scattering light in the leaves, confer mechanical support and tissue rigidity, and facilitate pollen release, germination, and tube growth (Bauer, Elbaum, & Weiss, 2011; Currie & Perry, 2007; Gal, Brumfeld, Weiner, Addadi, & Oron, 2012; He et al., 2014; Horner, 2012; Horner & Wagner, 1992; Iwano, Entani, Shiba, Takayama, & Isogai, 2004; Kuo-Huang, Ku, & Franceschi,

wileyonlinelibrary.com/journal/gbi

2007; Pritchard, Prior, Rogers, & Peterson, 2000). In addition to these physiological functions, plant biominerals have also ecological significance. Indeed, several studies reported that they may play a role in the protection of plants against herbivores and phytopathogens (Currie & Perry, 2007; Franceschi & Nakata, 2005; Lins, Barros, da Cunha, & Miguens, 2002; Nakata, 2012). Furthermore, biomineralization processes in plants are involved in the biogeochemical cycles of calcium, silicon, and in a lower degree in the cycle of carbon with the sequestration of atmospheric CO_2 (Braissant, Cailleau, Aragno, & Verrecchia, 2004; Cailleau, Braissant, & Verrecchia, 2011; Conley, 2002; Cornelis, Ranger, Iserentant, & Delvaux, 2010; Dauer & Perakis, 2014; Meunier et al., 2010; Tooulakou et al., 2016; Van Cappellen, 2003).

The most common biominerals in plants are calcium oxalate crystals (CaOxs), amorphous silica, and calcium carbonate (calcite, aragonite, vaterite, amorphous $CaCO_3$) (Bauer et al., 2011). To a lesser extent, other biominerals have been reported in some plant species such as calcium sulfate, calcium phosphate, calcium citrate (earlandite), calcium tartrate, calcium malate, magnesium oxalate (glushinkite), strontium sulfate, and barium sulfate (He et al., 2014; Monje & Baran, 2005). In addition, those biominerals can also entrap heavy metals such as aluminum, iron, cadmium, strontium, and zinc into their crystal structure, making the diversity of biominerals even more important (He, Bleby, Veneklaas, Lambers, & Kuo, 2012a,b; He et al., 2014; Sarret et al., 2006, 2007).

Notably, biominerals have been found in leaves, roots, stems, barks, flowers, fruits, and seeds as intra- and/or extracellular coating layers (Bouropoulos, Weiner, & Addadi, 2001; Currie & Perry, 2007; Franceschi & Nakata, 2005; Ilarslan, Palmer, & Horner, 2001; Lins et al., 2002; Morgan-Edel, Boston, Spilde, & Reynolds, 2015; Webb, 1999). Several studies focusing on the morphology and the distribution of biominerals reported that different plant species or genera harbored different crystal macropatterns, suggesting that the crystal deposition is a genetically controlled process which is species dependent (Horner, Wanke, & Samain, 2012; Lersten & Horner, 2000, 2011). The use of these biominerals as a taxonomic tool based on crystal types and their macropatterns was even proposed (Pennisi & McConnell, 2001; Prychid, Furness, & Rudall, 2003; Prychid & Rudall, 1999).

Among those biominerals, CaOxs are the most widespread in plants as they occur in about 75% of angiosperms (Franceschi & Horner, 1980; Nakata, 2012). In plants, CaOx can represent up to 80% of the plant's total dry weight, and up to 90% of the total content of calcium of the plant (Franceschi & Nakata, 2005; Webb, 1999; Zindler-Frank, 1976). They can be encountered in two hydrated forms in plants depending on the relative concentration of calcium and oxalic acid. The first corresponds to the monohydrate form and is called whewellite ($CaC_2O_4 \cdot H_2O$), while the second corresponds to the dehydrate form and is called weddellite ($CaC_2O_4 \cdot 2H_2O$) (Arnott, Pautard, & Steinfink, 1965; Bouropoulos et al., 2001; Frey-Wyssling, 1981). The formation of CaOx mostly occurs inside the vacuoles of specialized cells called idioblasts (Arnott, 1982; Foster, 1956). Plant CaOx is classified into five categories based on their morphology: prisms, druses, styloids, raphides, and crystal sand (Franceschi & Horner, 1980).

Silicon (Si) is a ubiquitous element in the plant kingdom with large variations of concentrations among plant lineages. According to the literature, Si accumulation is higher in monocotyledons, especially in Poaceae, with 1%–15% of shoot dry weight, than in dicotyledons where Si represents less than 0.5% of shoot dry weight (Conley, 2002). Amorphous silica is slightly soluble and occurs mostly as opal ($SiO_2 \cdot nH_2O$) in plants. Within the plant, amorphous silica is deposited in specialized cells called phytoliths (Bauer et al., 2011).

Although several studies reported the presence of biominerals in plants, most of them focused only on the observation and analysis of the spatial distribution of a single type of biomineral in a single tissue or at the whole plant scale. Consequently, our understanding of the actual diversity and chemical characteristics of plant biominerals and their relative abundance in plant tissues remains largely unknown. In this context, our study focused on i) identifying the morphology, distribution, and relative abundance of biominerals in two tree species (i.e., beech and sycamore maple) and specifically on different plant compartments (foliage, branch, trunk, and root) using scanning electron microscopy (SEM) and X-ray microcomputed tomography (XMCT) approaches, ii) determining the chemical composition of all the types of biominerals detected by X-ray diffraction (XRD) and energy-dispersive X-ray (EDX) spectroscopy analyses, iii) quantifying those biominerals in the different compartments by inductively coupled plasma-atomic emission spectroscopy (ICP-AES), and iv) modeling the representativeness of these biominerals at the scale of the tree and of the forest stand.

2 | MATERIALS AND METHODS

2.1 | Site description

The study was conducted in the deciduous high forest of Montiers, located in the northeastern of France (48°31′N, 5°16′E, altitude 340–386 m above sea level). This site is jointly managed by INRA-BEF (French National Institute for Agricultural Research—Biogeochemical cycles in Forest Ecosystems Research Unit, https://www6.nancy.inra.fr/bef) and ANDRA (French National Radioactive Waste Management Agency). The climate is semicontinental, with mean annual temperature of 12.6°C (monthly averages ranking from 4.4 to 21.2°C) and mean annual rainfall of 1100 mm. The stand is composed of beech (*Fagus sylvatica* L., 88%), sycamore maple (*Acer pseudoplatanus* L., 6%), and other deciduous trees (6%). Due to the forestry practices, all the trees were approximately 55 years (average age) in 2014. The studied Montiers site covers approximately 73 ha and is composed of three successive soil types: Alocrisol, Calci-brunisol, and Rendisol (AFES, 2009) or Distric Cambisol, Eutric Cambisol, and Rendzic Leptosol (IUSS Working group WRB, 2014) which represent about 30%, 50%, and 20% of the surface area of the forest site *(http://www.nancy.inra.fr/en/Outils-et-Ressources/montiers-ecosystem-research)*.

2.2 | Sampling procedure

To integrate the diversity of ecological factors in the Montiers site, two sampling collections were performed. All vegetative compartments

(foliage, branch, trunk, and root) of trees were sampled in trees growing in the different soil types occurring along the Montiers site.

During the first collection in 2010, six trees (three beeches and three sycamore maples) sharing similar tree diameters at breast height (DBH) measured at 1.30 m aboveground were harvested from the different soil types of the Montiers site by cutting at approximately 10 cm above the ground line. Each trunk was cut using a chain saw, and trunk sections were then intersected with a circular saw to avoid contamination with chainsaw oil. For each tree, fresh trunk sections at 1.30 m aboveground were divided into bark and wood. All samples were dried at 65°C in a drying oven for at least 1 week or until they reached constant weight. These trunk samples were used for the observation of biominerals.

In the same way, a selection of six trees (three beeches and three sycamore maples) sharing similar tree DBH were harvested during the second collection in February 2014 as described before. Several compartments of these six trees were used for the observation of biominerals (i.e., litterfall leaves, branch, trunk, and root) and chemical measurements (i.e., fresh leaves, branch, and trunk). For each tree, samples of trunk at 1.30 m aboveground (bark and wood), branch (bark and wood), and fine roots (diameter less than 5 mm) were collected. Trunk samples were prepared using the same protocol as in the first sampling collection. Small branches were cut using a chain saw, and to avoid sample contamination with chainsaw oil, they were then intersected with clean pruning shears and divided into bark and wood. For the foliage, two types of samples were collected: (i) fresh leaves for chemical measurements and (ii) litterfall leaves for SEM observations and calculation of the biomass. In August 2013, fresh leaves were collected from trees developed on different soil types by shooting off small branches with a shotgun. Litterfall leaves of the same species were collected through 18 L bags (each one with a surface of 0.58 * 0.58 m^2) per soil type during 8 weeks in December 2013 and then sorted out by species. Roots were collected by digging a hole at the foot of each tree. Roots were first rinsed with tap water before being cleaned off all substrate particles using ultrapure water and the Mini Piezon Dental Ultrasonic Scaler System (EMS, Switzerland). All samples were dried at 65°C for at least 1 week or until they reached constant weight. Finally, all samples were divided into two subsamples: A subsample of each sample was used for SEM and XMCT analyses, and the remaining subsamples were weighed and milled in a tungsten carbide mill bowl (Sodemi, France) to produce a homogenized powder (2-mm mesh) for XRD analyses and for the chemical analyses as described later.

2.3 | Preparation of samples for scanning electron microscopy (SEM)

Wood radial sections and cross sections of roots, litterfall leaves, and bark were mounted on aluminum stubs using double-coated carbon conductive tabs and covered with carbon. Samples were examined at the GeoRessources Laboratory (University of Lorraine) for biomineral occurrence and composition using a Hitachi S-4800 scanning electron microscope equipped with an energy-dispersive X-ray spectroscopy (EDX) containing a lithium-drifted silicon detector. SEM analyses were

carried out using an acceleration voltage of 10 or 15 kV with a working distance of 15 mm and with an average dead time of 100 seconds.

2.4 | Analyses of the mineralogical composition

The 2-mm powder samples of fresh leaves, root, bark, and wood from trunk and branch were mounted on a glass sample holder and placed directly in the diffractometer. XRD analyses were performed with a Siemens D5000 diffractometer equipped with a graphite monochromator, using Cu-Kα radiation. A first batch of samples was analyzed within the range 2.5–70° 2-theta with the following setup: a 0.01° 2-theta step, a counting time of 3 seconds per step, X-ray generator was operated at 40 kV and 20 mA. Because no peak was detected beyond 40° 2-theta, the remaining samples were analyzed within the range 2.5–40° 2-theta with the same setup. X-ray powder diffractograms were numerically recorded by a DACO-MP recorder associated with a microcomputer using the DIFFRAC-AT software (Socabim, France). The mineralogical composition of each sample was determined by comparing diffraction patterns of the samples with reference patterns of the American Society for Testing and Materials (ASTM) software.

2.5 | X-ray microcomputed tomography analysis (XMCT)

The distribution of calcium mineralization in roots, branches, and trunk of beech and sycamore maple trees was investigated by XMCT analyses using a nanotom 180 kV/15 W Phoenix-GE microtomograph at the GéoRessources laboratory (University of Lorraine). The XMCT method is non-destructive and permits acquiring three-dimensional images of solid samples. The analyzed samples were mounted with aluminum foil on a glass holder. The distances between the X-ray source from the detector and between the X-ray source and the sample were 20 mm and 400 mm, respectively. The data acquisition was performed at an acceleration voltage of 105 kV and a beam current of 90 μA. The images acquired after a full 360° rotation had a voxel size of 2.5 μm^3. The three-dimensional reconstruction of the sample was performed by the VGStudio Max 2.2 software and processed with Gauss filter, and the images were post-processed with FEI Avizo Fire 9.0 software. Quantification of calcium mineralization was performed on the trunk of both tree species developed on Rendisol (Rendzic Leptosol, IUSS Working Group WRB, 2014). Three regions corresponding to the bark, bark/sapwood interface, and sapwood were investigated. Total matter (i.e., matter detected by the tomograph, sum of wood matter, and calcium mineralization), wood matter, and calcium mineralization were quantified as volumes and then expressed as percentage of total matter volume.

2.6 | Analyses of the chemical composition and biomineral concentration in tree compartments

Total calcium (Ca$_{tot}$) and total silicon (Si$_{tot}$) composition of the samples (0.2 g for each powder sample of fresh leaves, bark, and wood of trunk and branch) was determined with an inductively coupled plasma-atomic

emission spectroscopy (ICP-AES), after alkaline fusion with 0.6 g of $LiBO_2$ and dissolution in HNO_3 during one night under magnetic stirring at the laboratory SARM (CNRS, Vandœuvre-lès-Nancy).

Total oxalic acid content in fresh leaves, trunk, and branch (wood and bark) samples was assessed by colorimetric enzyme assay using the clinical urinalysis kit (Libios SARL, Pontcharra sur Turdine, France). This test is based on the oxidation of oxalic acid into carbon dioxide and hydrogen peroxide by oxalate oxidase. Then, the hydrogen peroxide reacts with 3-methyl-2-benzothiazolinone and 3-(dimethylamino)-benzoic acid in the presence of peroxidase to yield an indamine dye which has an absorbance maximum at 590 nm. The intensity of the color is directly proportional to the oxalic acid concentration in the sample. This method is linear up to 1 mM, and the limit of detection is 0.07 mM.

To measure total oxalic acid content, 0.1 g of powder sample was added to 25 ml HCl 1N to dissolve the CaOx. Reactions were set for 16 h under gentle agitation at room temperature. Then, the pH of the solution was adjusted to 2 with HCl 30%. Oxalic acid concentration in each sample was determined using the oxalate-100 kit (Libios SARL, Pontcharra sur Turdine, France) following the supplier's recommendations. Absorbance was read at 590 nm in a Bio-Rad iMark Microplate Absorbance Reader (Bio-Rad, Hercules, California, USA). To estimate the amount of calcium present in the form of CaOx in this study, we considered that all of the oxalic acid content was bound to calcium and present as calcium oxalate in the tree compartments. The amount of whewellite ($CaC_2O_4 \cdot H_2O$) in different samples was directly determined from total oxalic acid content using a molar mass ratio of 1.62. The quantity of opal (empirical formula: $SiO_2 \cdot 1.5H_2O$) in both tree species was calculated from Si_{tot} concentrations using a molar mass ratio of 2.78. Calcium as the oxalate form (Ca_{ox}) in CaOx is considered here as whewellite and was calculated from CaOx formula with a molar mass ratio of 0.27.

2.7 | Calculation of the biomass of leaves, trunk, and branch

The biomass of leaves was assessed through the follow-up of annual leaf falls. Litterfall leaves were first dried at 65°C during at least 1 week and weighed. These quantities have been extrapolated for a surface area of one hectare giving thus, for each soil, the amount of leaves per hectare.

Tree aboveground biomass (trunk and branch) was estimated from measurements of height, diameter at breast level, age of trees and from the use of allometric equations linking dendrometric measurements and age of trees to the biomass (Genet et al., 2011; Picard, Saint-Andre, & Henry, 2012):

$$Y_{i,j} = \alpha_j + \beta_j \times (d^2h)^{\gamma_j} + \sigma \times (d^2h)^k \tag{1}$$

where Y is the independent variable, that is, the biomass (in metric tons of dry matter by hectare) for a given compartment i on a given soil j; d is the diameter at breast height in m; h is the total tree height in m; α, β, γ are the model parameters to be estimated; and $\sigma \times (d^2h)^k$ is

the error term accounting for the unexplained variance, σ following a normal law of mean zero and variance 1.

The parameters of these equations were defined for the Montiers site for beech and sycamore maple and for each tree compartment (i.e., branch <4 cm in diameter, branch between 4 and 7 cm in diameter, branch > 7 cm in diameter, stem wood, stem bark) (Genet, 2010; Saint-André et al., 2014). To obtain the total aboveground biomass of the Montiers site, equation (1) was also applied to the other tree species present in the study site.

2.8 | Amount of biominerals in trees

For each soil type, biomineral amounts were assessed in the different compartments of trees on the basis of one hectare as follows:

$$M_Bx = (([E]x * BMx)/1000) * MM_B/MM_E \tag{2}$$

with M_Bx the mass of the biomineral B (in kg/ha) in the compartment x, $[E]x$ the concentration (in g by kg of dry matter) of the element E in the compartment x, BMx the biomass (in kg of dry matter) of the compartment x, MM_B the molar mass of the biomineral, and MM_E the molar mass of the element.

For each soil type, the total biomineral content in the aboveground tree was obtained by adding the biomineral content of all compartments. Then, the biomineral content in the aboveground tree biomass of the Montiers site was determined by integrating the relative surface of the different soil types, that is, 30%, 50%, and 20% for the Alocrisol (Distric Cambisol), Calci-brunisol (Eutric Cambisol), and Rendisol (Rendzic Leptosol), respectively.

2.9 | Statistical analysis

The unpaired t-test was used to evaluate the significance of the differences between species in individual plant compartments.

3 | RESULTS

3.1 | Morphology, distribution, and crystal relative abundance

Based on SEM and XMCT analyses, six different shapes of crystals (i.e., prism, druse, raphide, octahedral, spherical, and crystal coating layers [CCLs]) were found in the different tree compartments of beech and sycamore maple. The description of the different biomineral types detected, their spatial distributions, and their relative abundance is presented in Table 1. Given that the branch and trunk shared exactly the same crystal macropattern, these two compartments have been treated together in this study. In both tree species, prisms, druses, and CCLs were the three most common crystal types (Figures 1–3).

Prisms were seen in all investigated compartments and shared a common spatial distribution whatever the tree species is (Table 1, Figures 1c,g, 2b,e, 3a,e,h,l,m). In contrast, distribution pattern of druses was totally reversed in beech when compared to the sycamore maple (Table 1, Figures 1f, 2a, 3a,e,i,k). The third most common shape

TABLE 1 Crystal types, occurrence, and relative abundance in root, leaves, trunk and branch of beech and sycamore maple

Biominerals	*Fagus sylvatica* L. (beech)	*Acer pseudoplatanus* L. (sycamore maple)
Calcium oxalate		
Prisms	R: lower cortex (fig. 1C) +++ L: vascular bundles (fig. 2B) +++ T & B: cortical parenchyma (fig. 3A, 3E) +++ T & B : vessel element in heartwood and sapwood (fig. 3L) rare	R: lower cortex (fig. 1G) + L: vascular bundles (fig. 2E) +++ T & B: cortical parenchyma (fig. 3H) +++ T & B: vessel element in heartwood and sapwood (fig. 3M) rare
Druses	L: palisade mesophyll cells (fig. 2A) + L: spongy mesophyll cells + T & B: cortical parenchyma (fig. 3A, 3E) +++ T & B: pith (fig. 3K, 3I) +	R: lower cortex (fig. 1F) +
Raphides	n.d.	R: lower cortex (fig. 1H, 1I) +
Octahedral	n.d.	R: lower cortex (fig. 1H) + R: medullary parenchyma (fig. 1K) +
Spherical	n.d.	R: medullary parenchyma (fig. 1J) +
Amorphous silica		
Spherical	n.d.	L: spongy mesophyll cells (fig. 2H) +
Si/O +/- (Ca and/or K) CCL	R: upper cortex (fig. 1D) +++ L: epidermis (fig. 2D) + L: vascular bundles (fig. 2C) + T & B: cork (fig. 3C) +++	L: epidermis (fig. 2G) ++ L: palisade mesophyll cells (fig. 2F) ++ L: spongy mesophyll cells (fig. 2H) + L: vascular bundles (fig. 2I) + T & B: cork (fig. 3F) +++
Other biominerals		
Spherical crystals of O/P/Mg/Ca/K	R: ray cells (fig. 1E) +	R: ray cells (fig. 1O) +
Spherical crystals of O/P/K/Mg/Na	n.d.	R: medullary parenchyma (fig. 1N) rare
O/K/Mg/Na and (Ca or S) CCL	n.d.	R: upper cortex (fig. 1L) +
K/O/Mg CCL	n.d.	R: upper cortex (fig. 1M) +
O/P/Ca/Mg/K CCL	T & B: collenchyma (fig. 3D) ++	n.d.
O/Ca/K/Mg +/- (S or P) CCL	n.d.	T & B: collenchyma (fig. 3G) ++

R, root, L, leaves, T & B, trunk and branch; CCL, crystal coating layer. Relative abundance: (+++) high, (++) medium, (+) low, (rare) sporadic.

TABLE 2 Average element concentrations in the tree organs of the investigated beeches and sycamore maples: mean values ± standard deviation

	Oxalic acid (mg g^{-1})		Ca as CaOx (mg g^{-1})		Ca$_{tot}$ (mg g^{-1})		Si$_{tot}$ (mg g^{-1})	
	Beech	Sycamore	Beech	Sycamore	Beech	Sycamore	Beech	Sycamore
Trunk Bark	55.2 ± 8.1	59.4 ± 24.4	24.6 ± 3.6	26.4 ± 10.9	26.8 ± 4.7	28.9 ± 8.6	2.6 ± 0.9	1.6 ± 0.4
Trunk Wood	<LD	<LD	<LD	<LD	1.3 ± 0.2	1.1 ± 0.1	0.05 ± 0.05	0.03 ± 0.03
Leaves	14.6 ± 1.2	21.8 ± 14.0	6.5 ± 0.5	9.7 ± 6.2	9.6 ± 1.2	14.1 ± 4.0	3.5 ± 1.5	6.4 ± 2.0
Branch Bark	70.0 ± 5.6 *	53.1 ± 11.2 *	31.1 ± 2.5*	23.6 ± 5.0*	31.0 ± 2.2	27.9 ± 3.8	2.1 ± 0.3 **	3.2 ± 0.5 **
Branch Wood	<LD	<LD	<LD	<LD	1.9 ± 0.5	2.0 ± 1.4	0.08 ± 0.05	0.03 ± 0.03

Total Ca and Si concentrations were determined after alkaline fusion with LiBO$_2$ and dissolution in HNO$_3$. Acid oxalic concentrations were determined by colorimetric enzyme assays. Ca as CaOx concentrations were calculated from oxalic acid concentrations.
Asterisks denote significant differences (**$p < .05$, *$p < .10$) between species ($n = 3$) according to the unpaired t test. <LD: below limit of detection.
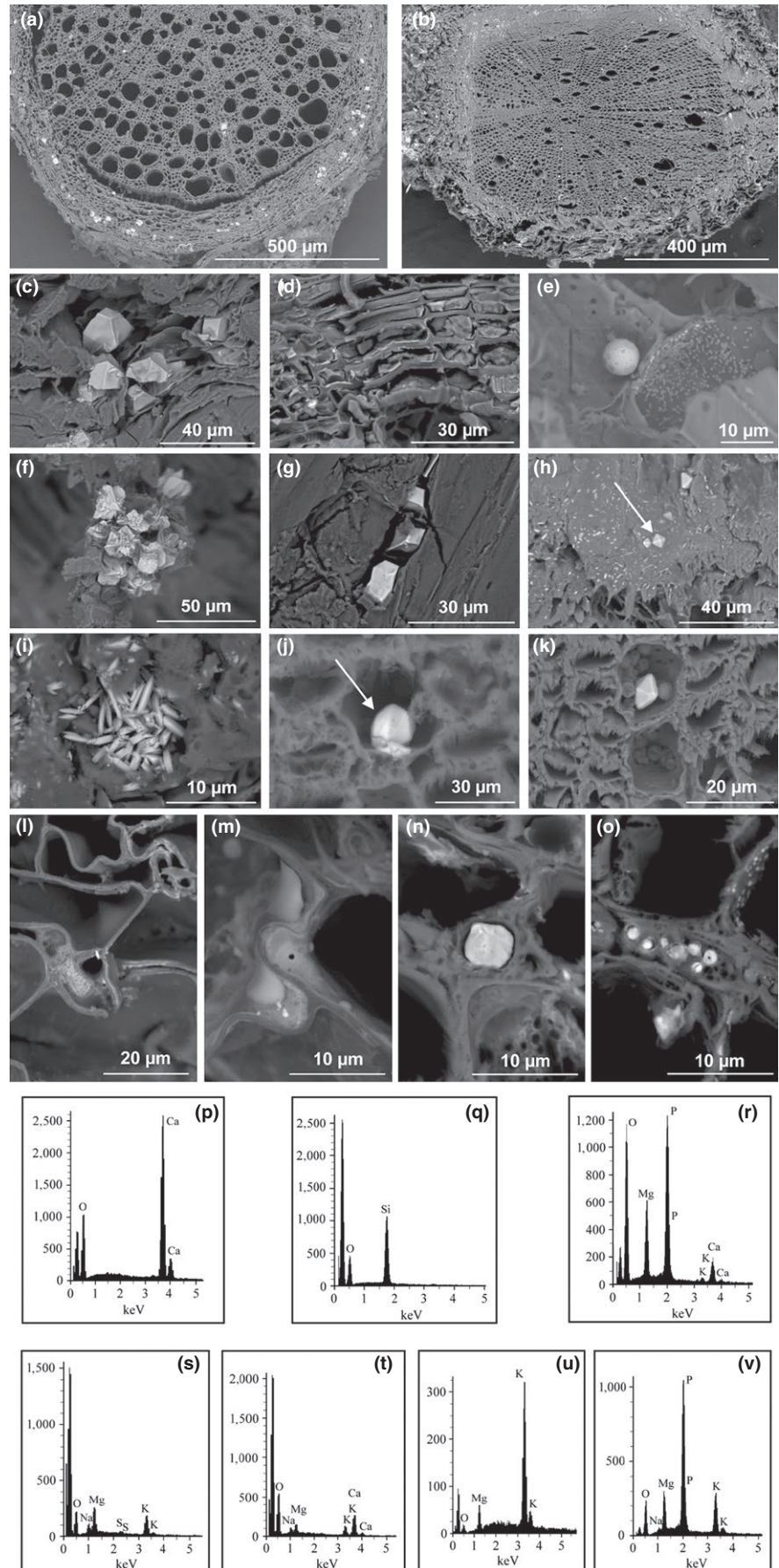
FIGURE 1 Diversity of biominerals in roots of beech and sycamore maple. (a–o) Scanning electron micrographs. (p–v) Energy-dispersive X-ray microanalysis (EDX) spectra of biominerals. Unlabeled peak at 0.277 keV corresponds to carbon K-alpha. (a) Part of a root cross section of beech. (b) General view of a root cross section of sycamore maple. (c) Cluster of calcium oxalate crystals in lower cortex of beech. (d) Part of a root cross section of beech showing a large amount of silicified layers in cells of upper cortex. (e) Spherical biomineral found in ray cells of beech. (f-k) Shape diversity of calcium oxalate crystals found in sycamore maple. (l, m) Layers of biominerals found in upper cortex of sycamore maple. (n, o) SEM micrographs of biominerals found in medullary parenchyma (n) and ray cells (o) in a root of sycamore maple. (p) Spectrum of calcium oxalate. (q) Spectrum of amorphous silica. (r) Corresponding EDX spectrum of spherical biomineral in (e, o). (s, t) Corresponding EDX spectra of biomineral layer in (l). (u) Spectrum of biomineral layer in (m). (v) Corresponding EDX spectrum of biomineral in (n)
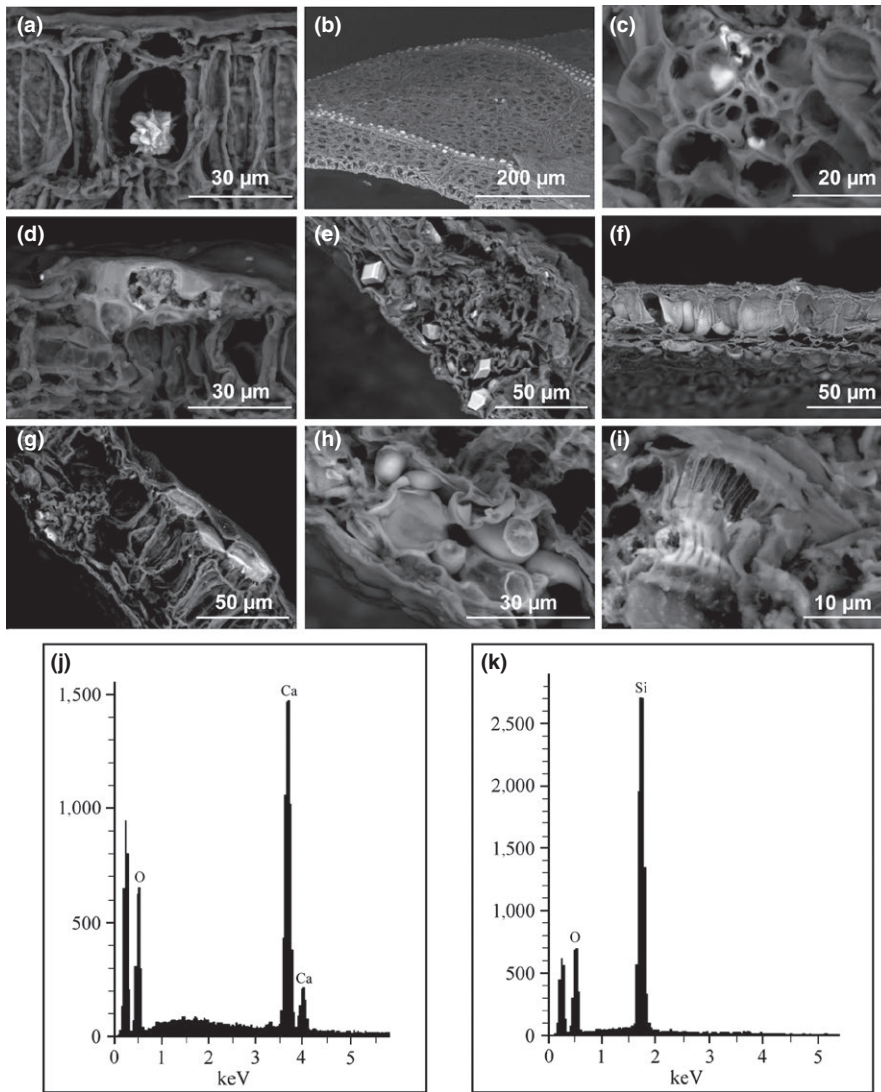
FIGURE 2 Diversity of biominerals in leaves of beech and sycamore maple. (a-i) Scanning electron micrographs. (j, k) Energy-dispersive X-ray microanalysis (EDX) spectra of biominerals. Unlabeled peak at 0.277 keV corresponds to carbon K-alpha. (a, b) Part of a cross section of a leaf of beech showing calcium oxalate as druse and prisms, respectively. (c, d) Amorphous silica in epidermis cells and around vascular bundles of beech, respectively. (e) Calcium oxalate as prisms around vascular bundles of sycamore maple. (f-i) Amorphous silica in palisade mesophyll cells, epidermis, spongy mesophyll cells, and around vascular bundles of sycamore maple, respectively. (j) EDX spectrum of calcium oxalate (a, b, e). (k) Corresponding EDX spectrum of amorphous silica (c, d, f-i)

of crystals detected corresponded to CCL and was localized in all the compartments of both tree species but more abundant in sycamore maple (Table 1, Figures 1d,l,m, 2c,d,i, 3c,d,f,g).

Besides these three types of crystals, some spherical crystals were identified in the ray cells of roots with an equivalent relative abundance in both tree species (Table 1, Figure 1e,o), but they were also found in medullary parenchyma of roots (Figure 1n) and in spongy mesophyll cells of leaves of sycamore maple (Figure 2h). Finally, the last two types of crystals (raphide and octahedral) were only detected in sycamore maple roots (Table 1). Few raphides and octahedral crystals were seen in the lower cortex (Figure 1h,i), and some octahedral crystals occurred as well in medullary parenchyma (Figure 1j,k).

To complete this biomineral characterization, the distribution and relative abundance of calcium mineralization were investigated using XMCT acquisition (Figure 4, Figure S1, Figure S2). Calcium mineralizations appeared to be more abundant in cortical parenchyma of branches (Figure 4c,d, Figure S1a,b) and trunk (Figure 4a,b, Figure S2a,b) of both species. They were also found in large quantity in the lower cortex of beech roots (Figure 4e, Figure S1d) and in a smaller proportion in the lower cortex of sycamore maple roots (Figure 4f,

Figure S1d). Calcium mineralizations were identified to a lesser extent in medullary rays of heartwood and sapwood in branches (Figure 4c,d, Figure S1a,b) and trunk (Figure 4a,b, Figure S2a,b) of both species, in pith of beech branches (Figure 4c, Figure S1a) and sycamore maple (data not shown), and in pith of sycamore maple trunk (Figure S2d).

3.2 | Crystallochemistry of the biominerals

All types of crystals viewed by SEM were then analyzed for their elemental composition by EDX analyses (Figures 1p–v, 2j–k, and 3n–v, Table 1). All prisms, druses, raphides, octahedral, and spherical crystals found in the medullary parenchyma of sycamore maple roots showed peaks for Ca and O, indicating the presence of calcium oxalate and/or calcium carbonate (Figures 1p, 2j,r).

The other spherical crystals showed several EDX spectra (Figures 1r,v,2k). Spherical crystals that occurred in Figure 2h displayed EDX spectra with peaks for O and Si and were representative for amorphous silica (Figure 2k). The EDX spectra of the spherical biominerals found in Figure 1e,o showed peaks for O, P, Mg, Ca, and K
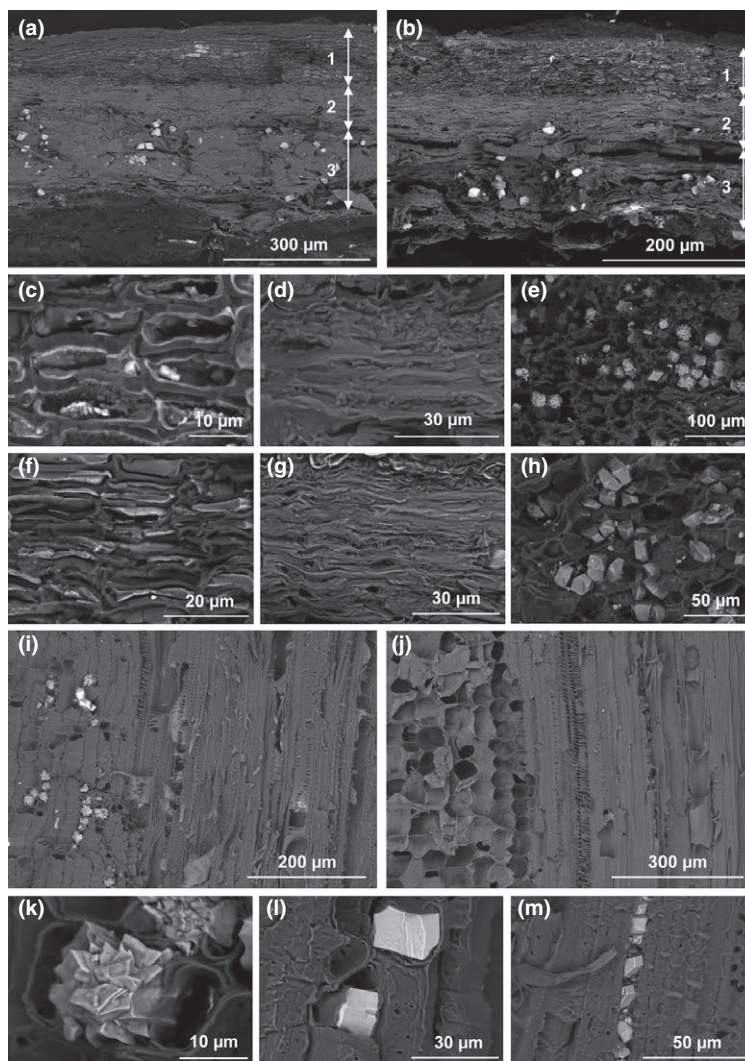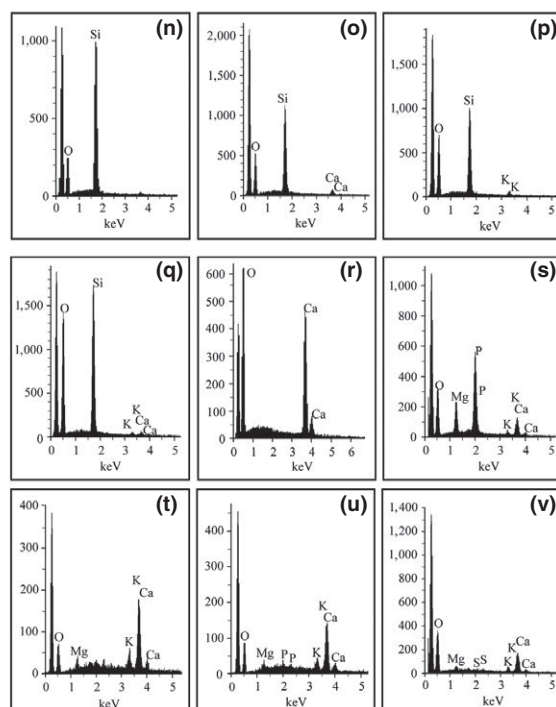
FIGURE 3 Diversity of biominerals in trunk and branches of beech and sycamore maple. (a-m) Scanning electron micrographs. (n-v) Energy-dispersive X-ray microanalysis (EDX) spectra of biominerals. Unlabeled peak at 0.277 keV corresponds to carbon K-alpha. (a) General view of the bark of a branch cross section of beech. (b) General view of the bark of a branch cross section of sycamore maple. (c, f) Part of a trunk cross section showing a large amount of silicified layers in bark of beech and sycamore maple, respectively. (d, g) Part of a branch cross section showing biominerals in collenchyma of beech and sycamore maple, respectively. (e, h) Shape diversity of calcium oxalate crystals found in cortical parenchyma of beech and sycamore maple, respectively. (i, j) General view of the pith and heartwood of a branch radial longitudinal section of beech and sycamore maple, respectively. (k-m) Shape diversity of calcium oxalate crystals found in pith and heartwood of beech (k, l) and in heartwood of sycamore maple (m). (n-q) Corresponding EDX spectra of amorphous silica found in bark of beech (n–p) and sycamore maple (q). (r) EDX spectrum of calcium oxalate (e, h, k-m). (s-v) Corresponding EDX spectra of biominerals layers found in (d, g)
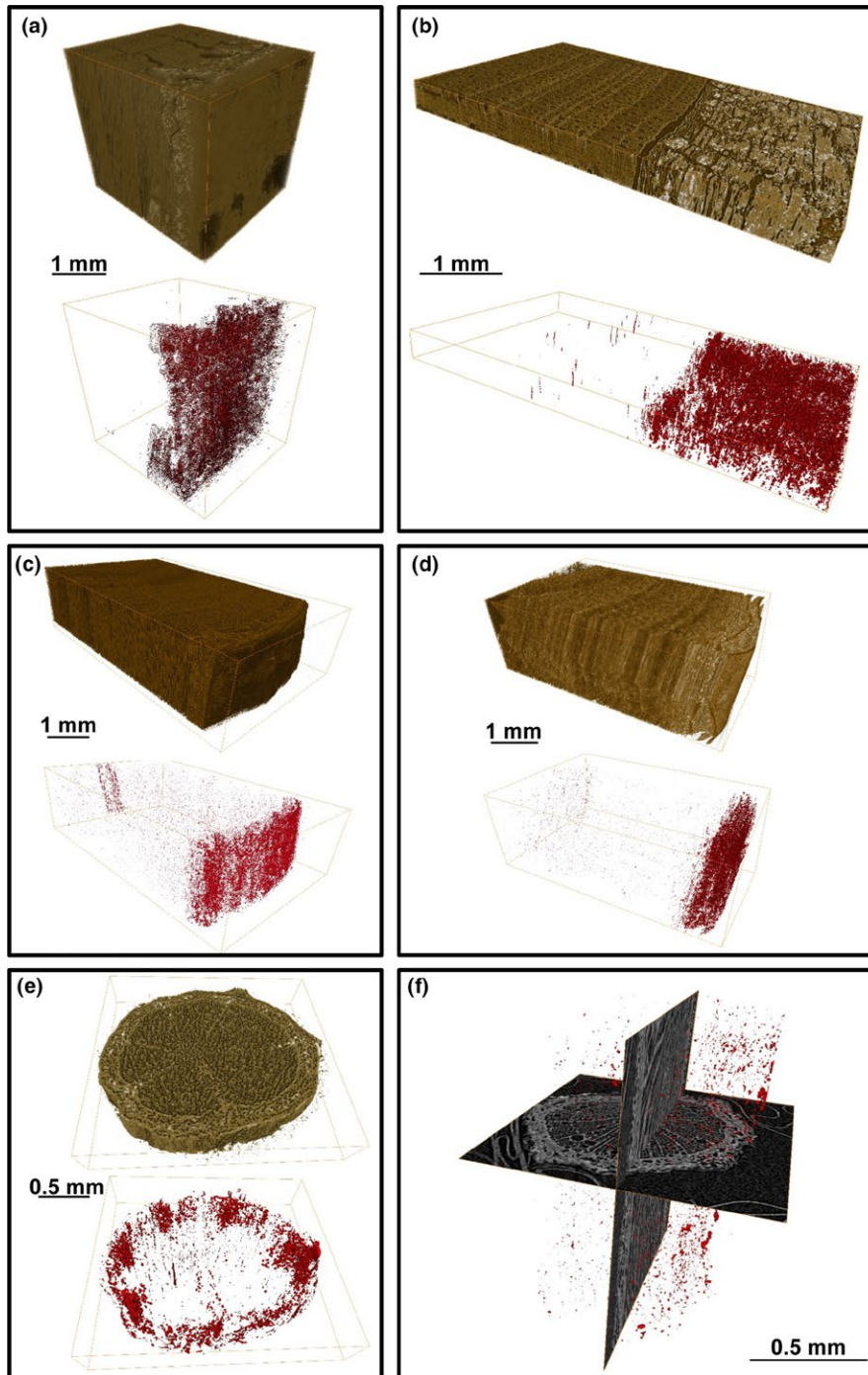
FIGURE 4 Three-dimensional imagery showing distribution of calcium mineralizations in beech and sycamore maple tissues. Beech sectional views of trunk (a), branch (c), and root (e). Sycamore maple sectional views of trunk (b), branch (d), and root (f). (a-e) On top: analyzed sample, on bottom: corresponding area showing calcium mineralizations (represented in red)

(Figure 1r) and were identical for the large spherical crystals (around 7 μm in diameter) and for small ones (<1 μm in diameter). Furthermore, the spherical crystals isolated in Figure 1n showed a similar EDX spectrum to those identified in ray cells except that the Ca was replaced by Na (Figure 1v).

EDX spectra revealed that most of CCLs were composed of amorphous silica whatever the compartment in beech and sycamore maple is (Table 1). CCLs in the upper cortex of beech (Figure 1d) and in leaves of both species (Figure 2c,d,f,g,i) had EDX spectra with peaks for O and Si and corresponded to amorphous silica (Figures 1q, 2k). Amorphous silica was also identified in the cork of both tree species (Figure 3c,f,n).

Notably, co-precipitation of Ca and/or K with amorphous silica was observed in cork tissues (Figure 3o–q).

Beyond calcium oxalate and silica, there were few other biomineral coating layers isolated in trunk and branches of both tree species (Table 1, Figures 1l, m,3d,g). The CCLs observed in trunk and branches of beech exhibited an identical EDX spectra to those obtained for the spherical crystals in ray cells of roots for both tree species and were composed of O, P, Ca, Mg, and K (Figures 1r, 3s). Similar EDX spectra were obtained for the CCLs in collenchyma of sycamore maple trunk and branches. These spectra showed peaks for O, Ca, K, and Mg (Figure 3t), and sometimes, a co-precipitation of S or P occurred
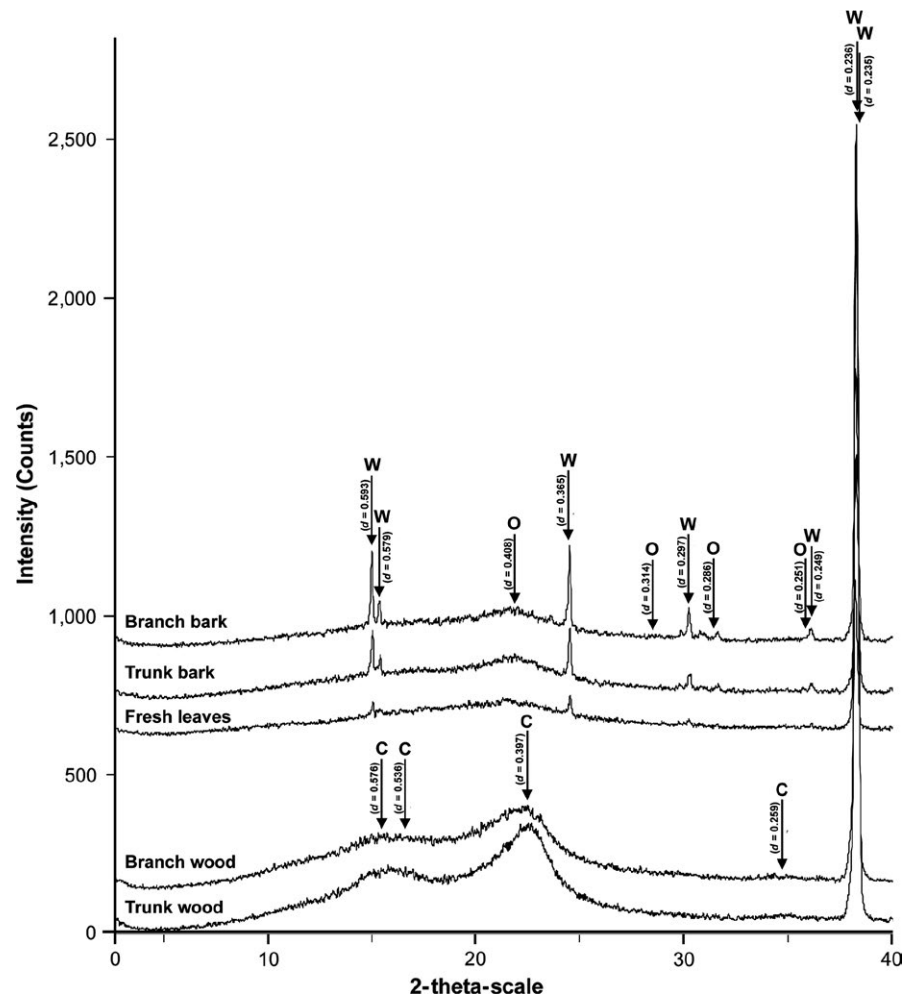
FIGURE 5 X-ray diffractograms from investigated compartments of beech and sycamore maple: branch bark (beech), trunk bark (beech), fresh leaves (sycamore maple), branch wood (beech), and trunk wood (beech). Identified minerals are presented with arrows. Numeric values correspond to interplanar spacing of the peaks, in nm. O: opal (00-038-0448), W: whewellite (00-020-0231), C: cellulose

(Figures 3u,v). Finally, CCLs isolated in Figure 1l,m exhibited EDX spectra with peaks for O, K, Mg (Figure 1u), and to a lesser extent peaks for Na, and Ca or S (Figure 1s,t). In addition, some Mn and Fe concentrations were observed in different tree compartments.

To complete the identification of all the components of the biomineral mixture, samples were analyzed by XRD. As there was no significant difference between beech and sycamore maple samples, only one representative sample for each studied tree compartment is given in Figure 5. The XRD analysis revealed the presence of two biominerals: whewellite ($CaC_2O_4 \cdot H_2O$) and opal (Figure 5) as suspected by EDX analysis. Notably, whewellite biominerals had the strongest intensity (discriminating peaks at 0.59, 0.37, and 0.24 nm) in all samples. Nevertheless, as opal is amorphous, most of its diffraction peaks (discriminating peaks at 0.29 and 0.25 nm) appeared only with a very weak intensity. Such results may be explained by the fact that biogenic opal produces broad and undefined peaks between 10° and 30° in the 2θ range (Kamatani, 1971; Lanning, Ponnaiya, & Crumpton, 1958). Furthermore, background level above which peaks are visible is quite high for wood samples and lower for leaves and bark samples and corresponds to a relative amount of amorphous content. This amorphous material (Figure 5) matched with the diffraction pattern of cellulose (discriminating peaks at 0.58 and 0.40 nm) as obtained by Oh and his collaborators (Oh et al., 2005). Altogether, our results showed, based

on the relative intensities of the diffraction peaks, only whewellite occurred in trunk and branch wood, whereas in fresh leaves and bark, whewellite was the main biomineral followed by opal.

3.3 | Quantification of the biominerals in the different tree compartments

The mean concentration of oxalic acid, Ca as calcium oxalate (Ca_{ox}), total Ca (Ca_{tot}), and total Si (Si_{tot}) in beech and sycamore maple compartments has been determined (Table 2). Trunk and branch wood concentrations were lower than trunk and branch bark concentrations for all elements. Based on the unpaired t-test, these results were not quantitatively different between beech and sycamore maple, except for oxalic acid, Ca_{ox}, and Si_{tot} in branch bark. Concerning Si, the largest amounts were found in the leaves of both species and their concentrations decreased in the following order for beech trees: fresh leaves > trunk bark > branch bark > branch wood > trunk wood, and their concentrations decreased in the following order for sycamore maple trees: fresh leaves > branch bark > trunk bark > branch wood = trunk wood (Table 2). Quantities of opal varied from 0% to 0.03% of dry weight for wood, from 0.25% to 0.77% of dry weight for bark, and from 0.5% to 1.8% of dry weight for leaves. Quantities of oxalic acid in both tree species were under detection limit in wood, and

concentrations of whewellite ranged from 6.2% to 14.0% for bark, and from 2.0% to 6.1% for leaves. At the forest stand scale, the amount of opal was estimated for leaves and for tree aboveground biomass in the Montiers forest and was 48 kg/ha and 123 kg/ha, respectively. In the same way, the amount of whewellite was calculated at the forest scale for leaves and for tree aboveground biomass and was 98 kg/ha and 1069 kg/ha, respectively.

To underpin the results for Ca, quantification of calcium mineralizations was assessed in the trunk at 1.30 m aboveground for beech and sycamore maple trees grown on Rendisol (Rendzic Leptosol) by XMCT analyses. For both tree species, three regions corresponding to the bark, bark/sapwood interface, and sapwood were investigated (Figure S2a,b). Quantification of calcium mineralizations by XMCT analyses in the trunk of both species indicated that calcium mineralizations were more abundant in bark (12.05% and 8.10% of total matter for beech and sycamore maple, respectively), followed by bark/wood interface (7.25% and 5.80% of total matter for beech and sycamore maple, respectively), and are scarce in sapwood (2.58% and 0.05% of total matter for beech and sycamore maple, respectively).

4 | DISCUSSION

The present study revealed the presence and relative distribution of biominerals were very similar in all the investigated tree compartments between both tree species. In both beech and sycamore maple, leaves and bark were rich in biominerals, whereas wood was quite poor in biominerals. This observation was consistent with the chemical analyses generated in our study or coming from other studies (Cornelis et al., 2010; Dauer & Perakis, 2014). For both tree species, biominerals were classified into three groups according to their crystallochemistry: (i) amorphous silica, (ii) calcium oxalate, and (iii) complex biominerals chemistry.

In our study, amorphous silica was mainly identified as pure opal in all investigated compartments based on the EDX analyses and XRD diffractograms. Such a result is coherent with previous studies performed on wheat, sorghum, corn, sunflower, and bamboo cane (Lanning et al., 1958; Lins et al., 2002). In addition to pure opal, opal with co-precipitations of Ca and/or K was also identified in the cork of both tree species (Figure 3c,f,o–q). This is coherent with the co-precipitations of Ca, K, and other elements to opal found in the cortex of *Matteuccia* roots and within the stem of *Eleocharis* (Channing & Edwards, 2003; Fu, Akagi, & Yabuki, 2002).

According to the literature, amorphous silica is supposed to occur mostly as coating layers in the leaf epidermis and in the cork of both tree species (Cornelis et al., 2010; Sommer et al., 2013), and in a lesser extent in the upper cortex of beech roots. As seen in Figure 3c,f, these silica coating layers occurred in the inner cell wall (Kim, Kim, Park, & Choi, 2002). However, some spherical particles of opal were observed in spongy mesophyll of sycamore maple leaves in the Montiers site.

The distribution of the opal in the different compartments of beech and sycamore maple trees seemed limited to the most external tissues of the trees in the Montiers site. Such localization is coherent

with previous studies and suggests that silica enhances plant resistance against insect herbivores and pathogenic micro-organisms by acting as a physical barrier to prevent penetration and by inducing plant defense responses (Cai, Gao, Chen, & Luo, 2009; Cai et al., 2008; Ma & Yamaji, 2006; Massey & Hartley, 2009).

In this study, biominerals containing Ca occurred almost exclusively as CaOx whatever the tree species is. Although two hydrated forms of CaOx have been described in other studies (Monje & Baran, 2005), only whewellite was identified in all investigated compartments of both tree species growing on the Montiers site. However, the presence of weddellite cannot be excluded due the precision (±5%) of the XRD method. Furthermore, our analyses did not permit to identify calcite whatever the tree compartment considered even if this biomineral has been described for other plants such as Cactaceae species and the tropical tree Iroko (Braissant et al., 2004; Monje & Baran, 2000). Such difference may be due to the plant species or may be related to the soil and climatic conditions in which such production has been observed.

Combination of all the methodologies developed in this study gave the nature, distribution, and quantities of biominerals in the different compartments of trees. These different tools allowed us to show that CaOxs are mostly found in the bark, in the cork, and in leaves of both tree species. However, although the XMCT technique is very integrative, small crystals remain difficult to identify and could explain why CaOxs identified by SEM observations in heartwood and pith of beech trunk were almost absent after XMCT analyses. Such a bias suggests that our analyses partly underestimated the real quantity of biominerals in trees.

CaOx observed in beech trees had two different shapes (prism and druse), whereas in sycamore maple, almost all major crystal types described so far were observed (prism, druse, octahedral, raphide, and spherical). The additional shapes found in sycamore maple were restricted to the roots. Reports of CaOx types in beech and sycamore maple tree species are very rare, and as far as we know, there is currently no study on the CaOx distribution pattern in the roots of these two deciduous species.

In both tree species, prisms occurred with a similar relative abundance in all compartments and were found in the lower cortex of roots, in vascular bundles of leaves, in the cortical parenchyma, and in the vessel element of heartwood and sapwood. In the literature, several authors already identified prisms in the wood parenchyma of several New Zealand *Fagus* tree species and in the trunk of *Trigonobalanus excelsa*, a member of the Fagaceae (Mennega, 1980; Patel, 1986), and in axial parenchyma of Korean Fagaceae and Aceraceae hardwood (Lee, Eom, & Chung, 1987). In this study, the distribution of druses differs largely between both tree species. In beech, druses were observed in palisade and spongy mesophylls of leaves and in cortical parenchyma and pith of trunk and branches, whereas in sycamore maple, druses were limited to the lower cortex of roots. Notably, Lersten and Horner (2008) also observed prisms and druses in vascular bundles, in palisade, and sometimes in spongy mesophyll among leaves of seven *Fagus* tree species.

CaOxs are suggested that they play a role in sequestrating the excess of calcium, detoxifying heavy metals, optimizing the

photosynthesis, participating in the plant defense against phytopathogen attacks, and conferring mechanical support and tissue rigidity (Franceschi & Nakata, 2005; Gal et al., 2012; He et al., 2014; Sarret et al., 2007). In all the compartments of these two tree species, the distribution of CaOx appeared to be associated with conductive tissues: CaOx occured mostly in axial phloem parenchyma cells in the trunk and branches, in the lower cortex of roots, and around the vascular bundles in leaves. The distribution of CaOx in beech and sycamore maple allowed us to hypothesize that in trunk, branches, and roots, CaOxs are mostly involved in the bulk calcium regulation but could also participate in tissue rigidity, whereas in leaves, prisms could play a role in the sequestration of excess of calcium and/or confer mechanic support in vascular bundles, and druses are most likely to contribute to the optimization of photosynthesis.

In addition to opal and CaOx, other types of more complex biominerals have been identified in beech and sycamore maple roots, trunk, and branches. These biominerals described for the first time in this study occurred as spherical crystals or as CCLs. Spherical crystals were specific to the roots of both tree species, whereas CCLs were found in root, trunk, and branches of sycamore maple trees, but were limited to the trunk and branches of beech trees. Among all these other biominerals, only one type was common to both tree species. They corresponded to spherical particles composed of O, P, Mg, Ca, and K which were found in the ray cells of roots. In both tree species, these biominerals varied in size, ranging from 0.5 to 7 μm in beech trees and 0.2 to 1.3 μm in sycamore maple trees. A closely related biomineral to the one mentioned above was found in the medullary parenchyma of sycamore maple roots, with the replacement of Ca by Na. Some CCLs were also found in the upper cortex of sycamore maple roots. They are composed of K, O, Mg and include sometimes Na, and Ca or S, making the biomineral diversity even greater. Finally, another biomineralized layer was identified in the cork of trunk and branches of both species between the opal and the CaOx layer. This layer corresponding to the collenchyma contained CCLs of O, Ca, K, and Mg with occasionally co-precipitations of S and P. Because this layer is very thin, it is difficult to determine whether this biomineral really corresponds to a mineral coating layer or whether this chemical composition corresponds to an enrichment in these elements of the underlying organic matter. Although the exact nature of these biominerals was not determined, to our knowledge, it is the first time that they are described.

Although several methods have been used to analyze total silicon in the literature, all the studies performed reported the same range of concentration for the silicon (Si_{tot}) in the leaves of European beech. In our study, a total amount of 3.5 ± 1.5 mg/g dry weight (dw) of Si_{tot} in leaves was obtained. This value appeared slightly lower than the total amount of silicon found in beech trees developed on soils rich in silicon (7.4 mg/g, Cornelis et al. (2010); 9.0 mg/g dw, Sommer et al. (2013)). Moreover, the Si_{tot} in trunk wood and trunk bark of Montiers site (0.05 mg/g dw and 2.6 mg/g dw, respectively) was slightly higher than Si_{tot} found by Cornelis et al. (2010) (0.02 mg/g dw and 1.5 mg/g dw, respectively) and Sommer et al. (2013) (0.02 mg/g dw and 2.6 mg/g dw, respectively).

Concerning Ca, our chemical analyses (Table 2) indicated that Ca_{tot} and Ca_{ox} concentrations were not equivalent among the different tree compartments, whatever the tree species considered: trunk wood < branch wood < fresh leaves < trunk bark < branch bark. Our results suggest that more the compartment is enriched in calcium, the higher the amount of Ca_{ox}. Such statement is supported by the linear relationship between Ca_{ox} and Ca_{tot} obtained for the trees analyzed. A detailed analysis of this relationship suggests that a part of Ca_{tot} occurs as free calcium or as calcium bound to the organic matter in the sample. As this relationship is valid whatever the compartments, the tree species, and the soil types are, our results suggest that CaOx precipitation seems to be controlled by the concentrations of Ca_{tot}. Such relationship was also observed for Douglas trees developed on two types of soils (rich and low in Ca; Figure 6; Dauer & Perakis, 2014). In this case, the linear relationship differed from the one obtained in our study, suggesting that the tree species and/or the climatic conditions determine the formation of CaOx. Although additional studies would be necessary for confirmation, these data suggest a biological control of CaOx precipitation as a regulation mechanism of bulk calcium or a chemical control based on solubility constants.

Trees contribute to the biogeochemical cycles of Si and Ca (Cornelis, Titeux, Ranger, & Delvaux, 2011; Dauer & Perakis, 2014; Sommer et al., 2013). At the forest stand scale, opal represents only 0.1% of the total aboveground biomass (123 kg/ha), but in leaves, this percentage raises up to 1.1% (48 kg/ha). Moreover, the amount of whewellite corresponds to 0.7% (1069 kg/ha) and 3.1% (98 kg/ha) of the total aboveground biomass and the total mass leaves, respectively. Although opal and whewellite represent a little percentage of the mass of compartments, the main part of Ca (Figure 6) and Si in trees is contained in these biominerals. Therefore, the precipitation of opal and whewellite in trees (171 and 1167 kg/ha) and their dissolution in litterfall impact the biogeochemical cycles of Si and Ca, respectively. Indeed, the biogenic production of Si as opal (48 kg.ha^{-1}.y^{-1}) in the Montiers site returns to soil solution after opal is dissolved in the litter layer. The biogenic production values of Si determined in our study are very similar to those assessed previously in beech forests in temperate climate in Europe (Cornelis et al., 2010; Sommer et al., 2013). Although silicon is widely present in soil minerals (McKeague & Cline, 1963) and is released into the soil solution by the weathering of silicate minerals, Sommer et al. (2013) demonstrated that it is the biogenic Si that contributes most to the Si dissolved in forest soils. In the same way, Ca is the element most recycled in forests (Fichter, Dambrine, Turpault, & Ranger, 1998). As Ca occurred mostly in the solid form in leaves (Figure 6, 98 kg.ha^{-1}.y^{-1}), the biogeochemical cycle of Ca is controlled by the precipitation of Ca in CaOx and by its transformation in the forest floor or in soil. Indeed, CaOx can be degraded into oxalate and Ca by micro-organisms (i.e., oxalotrophy), the oxalate can be used as a carbon source (Tamer & Aragno, 1980), and the remaining Ca is released in the soil solution. In some ecosystems such as tropical forests, Ca from CaOx can be precipitate as calcite in soil (Cailleau et al., 2011). This substantial impact of CaOx in the biogeochemical cycle of Ca was also clearly demonstrated in the Douglas forest ecosystem (Dauer & Perakis, 2014). Further studies are necessary to fully
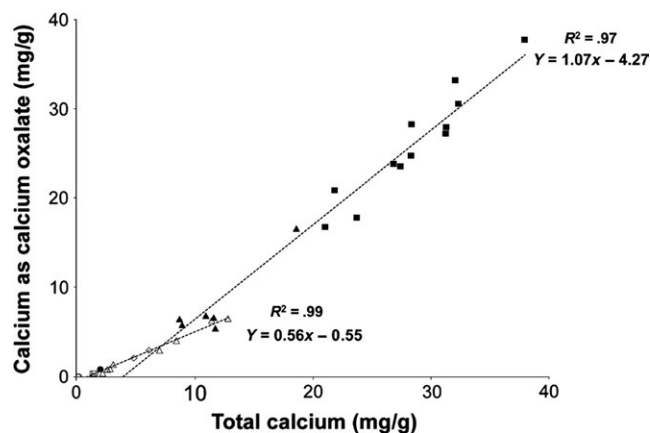
FIGURE 6 Regression lines between calcium as calcium oxalate concentrations and total calcium concentrations. ●: wood, ▲: fresh leaves, ■: bark in our study. ○: wood, △: fresh leaves, □: bark,◇: branches in Dauer & Perakis, 2014

understand how these biominerals precipitate within the trees and to determine their stability and their dynamics of formation. In addition to these two biominerals, the complex chemical biominerals identified in this study contribute also to the biogeochemical cycles of elements in the forest of Montiers, but further analyses are needed to estimate their significance.

5 | CONCLUDING REMARKS AND FUTURE DIRECTIONS

This study which aims at being integrative of all types of biominerals and of all types of compartments in deciduous trees showed a general distribution of biominerals within the trees independent of the species and soil types. Opal occurred as CCLs in the inner cell wall in most external tissues of the trees, suggesting a protective role, whereas whewellite, found mostly as prisms and druses, seemed to be associated with conductive tissues and could play a role in bulk calcium regulation and in the optimization of the photosynthesis efficiency. Spherical biominerals composed of complex elements were identified in ray cells of roots and could result from detoxification processes or storage forms. A strong correlation between Ca_{tot} and Ca_{Ox} was found in this study and in Dauer and Perakis (2014), but the equations of the regression lines differ. To identify which factors impact these equations, further work is needed using several tree species, different climatic conditions, and more extreme soil types. Many questions remain unanswered and should stimulate further research in the coming years. From the physiological point of view, further investigations are needed to determine the function of each biomineral and its dynamic of formation. The generalization of biomineral studies from additional tree species and ecological/climatic conditions is necessary to determine the ubiquitous and specific biominerals for each ecosystem. As a significant portion of the chemical elements occurred as biominerals, it is therefore necessary to develop calibrated methods to determine the different form of

elements in the tissues (i.e., soluble, bound to organic matter, contained in biominerals). These element speciations could allow for establishing in plants occurred general laws between total concentrations of each element and biomineral concentrations as seen in the relation between Ca_{tot} and Ca_{ox} in this study. From the biogeochemical point of view, the specific contribution of these biominerals could be included systematically in biogeochemical cycles notably during the organic matter recycling.

CONFLICT OF INTEREST

The authors declare no conflict of interest.

AUTHOR CONTRIBUTIONS

M.-P.T. conceived and conducted the design of the study, acquired data, and revised the manuscript. C.K. and C.C. analyzed and interpreted data. C.K. wrote the manuscript. L.S. prepared the samples and performed the SEM and EDX analyses. C.M. prepared the samples and performed the XMCT analyses. S.U. provided useful help for oxalic acid quantification. All authors read and approved the final manuscript.

REFERENCES

AFES (2009). *Référentiel pédologique 2008* (Editions Quae). Versailles: Quae.

Arnott, H. J. (1982). Three systems of biomineralization in plants with comments on the associated organic matrix. In G. H. Nancollas (Ed.), *Biological mineralization and demineralization* (pp. 199–218). Berlin Heidelberg: Springer.

Arnott, H. J., Pautard, F. G. E., & Steinfink, H. (1965). Structure of calcium oxalate monohydrate. *Nature, 208*, 1197–1198.

Bauer, P., Elbaum, R., & Weiss, I. M. (2011). Calcium and silicon mineralization in land plants: Transport, structure and function. *Plant Science, 180*, 746–756.

Bouropoulos, N., Weiner, S., & Addadi, L. (2001). Calcium oxalate crystals in tomato and tobacco plants: Morphology and *in vitro* interactions of crystal-associated macromolecules. *Chemistry, 7*, 1881–1888.

Braissant, O., Cailleau, G., Aragno, M., & Verrecchia, E. P. (2004). Biologically induced mineralization in the tree *Milicia excelsa* (Moraceae): Its causes and consequences to the environment. *Geobiology, 2*, 59–66.

Brown, S. L., Warwick, N. W. M., & Prychid, C. J. (2013). Does aridity influence the morphology, distribution and accumulation of calcium oxalate crystals in *Acacia* (Leguminosae: Mimosoideae)? . *Plant Physiology and Biochemistry : PPB*, *73*, 219–228.

Cai, K., Gao, D., Chen, J., & Luo, S. (2009). Probing the mechanisms of silicon-mediated pathogen resistance. *Plant Signaling & Behavior*, *4*, 1–3.

Cai, K., Gao, D., Luo, S., Zeng, R., Yang, J., & Zhu, X. (2008). Physiological and cytological mechanisms of silicon-induced resistance in rice against blast disease. *Physiologia Plantarum*, *134*, 324–333.

Cailleau, G., Braissant, O., & Verrecchia, E. P. (2011). Turning sunlight into stone: The oxalate-carbonate pathway in a tropical tree ecosystem. *Biogeosciences Discuss*, *8*, 1077–1108.

Channing, A., & Edwards, D. (2003). Experimental taphonomy: Silicification of plants in Yellowstone hot-spring environments. *Transactions of the Royal Society of Edinburgh, Earth Science*, *94*, 503–521.

Conley, D. J. (2002). Terrestrial ecosystems and the global biogeochemical silica cycle. *Global Biogeochemical Cycles*, *16*, 1121.

Cornelis, J.-T., Ranger, J., Iserentant, A., & Delvaux, B. (2010). Tree species impact the terrestrial cycle of silicon through various uptakes. *Biogeochemistry*, *97*, 231–245.

Cornelis, J.-T., Titeux, H., Ranger, J., & Delvaux, B. (2011). Identification and distribution of the readily soluble silicon pool in a temperate forest soil below three distinct tree species. *Plant and Soil*, *342*, 369–378.

Currie, H. A., & Perry, C. C. (2007). Silica in plants: Biological, biochemical and chemical studies. *Annals of Botany*, *100*, 1383–1389.

Dauer, J. M., & Perakis, S. S. (2014). Calcium oxalate contribution to calcium cycling in forests of contrasting nutrient status. *Fisheries Management and Ecology*, *334*, 64–73.

Fichter, J., Dambrine, E., Turpault, M.-P., & Ranger, J. (1998). Base cation supply in spruce and beech ecosystems of the Strengbach catchment (Vosges mountains, NE France). *Water, Air, and Soil pollution*, *104*, 125–148.

Foster, A. S. (1956). Plant idioblasts: Remarkable examples of cell specialization. *Protoplasma*, *46*, 184–193.

Franceschi, V. R., & Horner, H. T. Jr (1980). Calcium oxalate crystals in plants. *Botanical Review*, *46*, 361–427.

Franceschi, V. R., & Nakata, P. A. (2005). Calcium oxalate in plants: Formation and function. *Annual Review of Plant Biology*, *56*, 41–71.

Frey-Wyssling, A. (1981). Crystallography of the two hydrates of crystalline calcium oxalate in plants. *American Journal of Botany*, *68*, 130–141.

Fu, F., Akagi, T., & Yabuki, S. (2002). Origin of silica particles found in the cortex of roots. *Soil Science Society of America Journal*, *66*, 1265–1271.

Gal, A., Brumfeld, V., Weiner, S., Addadi, L., & Oron, D. (2012). Certain biominerals in leaves function as light scatterers. *Advanced Materials*, *24*, OP77–OP83.

Genet, A. (2010). Quantification of fuelwood potentials from French beech forests: updated allometric modeling tools and robustness to differences in soil fertility. Doctoral dissertation, Université Savoie Mont Blanc.

Genet, A., Wernsdörfer, H., Jonard, M., Pretzsch, H., Rauch, M., Ponette, Q., … Saint-Andre, L. (2011). Ontogeny partly explains the apparent heterogeneity of published biomass equations for *Fagus sylvatica* in central Europe. *Fisheries Management and Ecology*, *261*, 1188–1202.

He, H., Bleby, T. M., Veneklaas, E. J., Lambers, H., & Kuo, J. (2012a). Precipitation of calcium, magnesium, strontium and barium in tissues of four *Acacia* species (Leguminosae: Mimosoideae). *PLoS ONE*, *7*, e41563.

He, H., Bleby, T. M., Veneklaas, E. J., Lambers, H., & Kuo, J. (2012b). Morphologies and elemental compositions of calcium crystals in phyllodes and branchlets of *Acacia robeorum* (Leguminosae: Mimosoideae). *Annals of Botany*, *109*, 887–896.

He, H., Veneklaas, E. J., Kuo, J., & Lambers, H. (2014). Physiological and ecological significance of biomineralization in plants. *Trends in Plant Science*, *19*, 166–174.

Horner, H. T. (2012). Unusual pit fields in lowermost hypodermal cell walls and uppermost walls of photosynthetic crystal-containing palisade parenchyma cells in *Peperomia obtusifolia* leaves. *Annals of Botany*, *109*, 1307–1315.

Horner, H. T., & Wagner, B. L. (1992). Association of four different calcium crystals in the anther connective tissue and hypodermal stomium of *Capsicum annuum* L. (Solanaceae) during microsporogenesis. *American Journal of Botany*, *79*, 531–541.

Horner, H. T., Wanke, S., & Samain, M.-S. (2012). A comparison of leaf crystal macropatterns in the two sister genera *Piper* and *Peperomia* (Piperaceae). *American Journal of Botany*, *99*, 983–997.

Ilarslan, H., Palmer, R. G., & Horner, H. T. (2001). Calcium oxalate crystals in developing seeds of soybean. *Annals of Botany*, *88*, 243–257.

IUSS Working Group WRB. 2014. World Reference Base for Soil Resources 2014.

Iwano, M., Entani, T., Shiba, H., Takayama, S., & Isogai, A. (2004). Calcium crystals in the anther of *Petunia*: The existence and biological significance in the pollination process. *Plant and Cell Physiology*, *45*, 40–47.

Kamatani, A. (1971). Physical and chemical characteristics of biogenous silica. *Marine Biology*, *8*, 89–95.

Kim, S. G., Kim, K. W., Park, E. W., & Choi, D. (2002). Silicon-induced cell wall fortification of rice leaves: A possible cellular mechanism of enhanced host resistance to blast. *Phytopathology*, *92*, 1095–1103.

Kuo-Huang, L.-L., Ku, M. S. B., & Franceschi, V. R. (2007). Correlations between calcium oxalate crystals and photosynthetic activities in palisade cells of shade-adapted *Peperomia glabella*. *Botanical Studies*, *48*, 155–164.

Lanning, F. C., Ponnaiya, B. W. X., & Crumpton, C. F. (1958). The chemical nature of silica in plants. 1. *Plant Physiology*, *33*, 339–343.

Lee, P.-W., Eom, Y.-G., & Chung, Y.-J. (1987). The distribution and shape of crystals in the xylem of Korean hardwoods. *Journal of Korean Wood Science and Technology*, *15*, 1–11.

Lersten, N. R., & Horner, H. T. (2000). Calcium oxalate crystal types and trends in their distribution patterns in leaves of *Prunus* (Rosaceae: Prunoideae). *Plant Systematics and Evolution*, *224*, 83–96.

Lersten, N. R., & Horner, H. T. (2008). Crystal macropatterns in leaves of Fagaceae and Nothofagaceae: A comparative study. *Plant Systematics and Evolution*, *271*, 239–253.

Lersten, N. R., & Horner, H. T. (2011). Unique calcium oxalate "duplex" and "concretion" idioblasts in leaves of tribe Naucleeae (Rubiaceae). *American Journal of Botany*, *98*, 1–11.

Lins, U., Barros, C. F., da Cunha, M., & Miguens, F. C. (2002). Structure, morphology, and composition of silicon biocomposites in the palm tree *Syagrus coronata* (Mart.) Becc. *Protoplasma*, *220*, 89–96.

Ma, J. F., & Yamaji, N. (2006). Silicon uptake and accumulation in higher plants. *Trends in Plant Science*, *11*, 392–397.

Massey, F. P., & Hartley, S. E. (2009). Physical defences wear you down: Progressive and irreversible impacts of silica on insect herbivores. *Journal of Animal Ecology*, *78*, 281–291.

McKeague, J. A., & Cline, M. G. (1963). Silica in soils. *Advances in Agronomy*, *15*, 339–396.

Mennega, A. M. (1980). Wood structure of *Trigonobalanus excelsa* G Lozano-C., Hdz-C. & Henao (Fagaceae), Caldasia, 97–101.

Meunier, J. D., Kirman, S., Strasberg, D., Nicolini, E., Delcher, E., & Keller, C. (2010). The output and bio-cycling of Si in a tropical rain forest developed on young basalt flows (La Reunion Island). *Geoderma*, *159*, 431–439.

Monje, P. V., & Baran, E. J. (2000). First evidences of the bioaccumulation of α-quartz in Cactaceae. *Journal of Plant Physiology*, *157*, 457–460.

Monje, P. V., & Baran, E. J. (2005). Evidence of formation of glushinskite as a biomineral in a Cactaceae species. *Phytochemistry*, *66*, 611–614.

Morgan-Edel, K. D., Boston, P. J., Spilde, M. N., & Reynolds, R. E. (2015). Phytoliths (plant-derived mineral bodies) as geobiological and climatic indicators in arid environments. *New Mexico Geology*, *37*, 3–20.

Nakata, P. A. (2012). Plant calcium oxalate crystal formation, function, and its impact on human health. *Frontiers in Biology*, 7, 254–266.

Oh, S. Y., Yoo, D. I., Shin, Y., Kim, H. C., Kim, H. Y., Chung, Y. S., ... Youk, J. H. (2005). Crystalline structure analysis of cellulose treated with sodium hydroxide and carbon dioxide by means of X-ray diffraction and FTIR spectroscopy. *Carbohydrate Research*, 340, 2376–2391.

Patel, R. N. (1986). Wood anatomy of the dicotyledons indigenous to New Zealand 15 Fagaceae . *New Zealand Journal of Botany*, 24, 189–202.

Pennisi, S. V., & McConnell, D. B. (2001). Taxonomic relevance of calcium oxalate cuticular deposits in *Dracaena* Vand. ex L. *HortScience*, 36, 1033–1036.

Picard, N., Saint-Andre, L., & Henry, M. (2012). Manual for building tree volume and biomass allometric equations: from field measurement to prediction (Food and Agricultural Organization of the United Nations: Rome, Italy/Centre de Coopération Internationale en Recherche Agronomique pour le Développement: Montpellier, France) (www.fao.org/docrep/018/i3058e/i3058e.pdf).

Pritchard, S. G., Prior, S. A., Rogers, H. H., & Peterson, C. M. (2000). Calcium sulfate deposits associated with needle substomatal cavities of container-grown longleaf pine (Pinus palustris) Seedlings. *International Journal of Plant Sciences*, 161, 917–923.

Prychid, C. J., Furness, C. A., & Rudall, P. J. (2003). Systematic significance of cell inclusions in Haemodoraceae and allied families: Silica bodies and tapetal raphides. *Annals of Botany*, 92, 571–580.

Prychid, C. J., & Rudall, P. J. (1999). Calcium oxalate crystals in monocotyledons: A review of their structure and systematics. *Annals of Botany*, 84, 725–739.

Saint-André, L., Genet, A., Legout, A., Ranger, J., Wernsdörfer, H., Jonard, M., , ... Deleuze, C. (2014). Modèles de biomasse et de minéralomasse. Quelles avancées de la recherche? Pour quels usages à terme en gestion? *Rendez-vous Techniques*, 44, 43–56.

Sarret, G., Harada, E., Choi, Y.-E., Isaure, M.-P., Geoffroy, N., Fakra, S., ... Clemens, S., & Manceau, A. (2006). Trichomes of tobacco excrete zinc as zinc-substituted calcium carbonate and other zinc-containing compounds. *Plant Physiology*, 141, 1021–1034.

Sarret, G., Isaure, M.-P., Marcus, M. A., Harada, E., Choi, Y.-E., Pairis, S., ... Manceau, A. (2007). Chemical forms of calcium in Ca, Zn- and Ca, Cd-containing grains excreted by tobacco trichomes. *Canadian Journal of Chemistry*, 85, 738–746.

Sommer, M., Jochheim, H., Höhn, A., Breuer, J., Zagorski, Z., Busse, J., ... Kaczorek, D. (2013). Si cycling in a forest biogeosystem–the importance of transient state biogenic Si pools. *Biogeosciences*, 10, 4991–5007.

Tamer, A. U., & Aragno, M. (1980). Isolement, caractérisation et essai d'identification de bactéries capables d'utiliser l'oxalate comme seule source de carbone et d'énergie. *Bulletin de la Société des science naturelles de Neuchâtel*, 103, 91–104.

Tooulakou, G., Giannopoulos, A., Nikolopoulos, D., Bresta, P., Dotsika, E., Orkoula, M. G., ... Karabourniotis, G. (2016). "Alarm photosynthesis": Calcium oxalate crystals as an internal CO_2 source in plants. *Plant Physiology*, 71, 2577–2585.

Van Cappellen, P. (2003). Biomineralization and global biogeochemical cycles. *Reviews in Mineralogy and Geochemistry*, 54, 357–381.

Webb, M. A. (1999). Cell-mediated crystallization of calcium oxalate in plants. *Plant Cell*, 11, 751–761.

Zindler-Frank, E. (1976). Oxalate biosynthesis in relation to photosynthetic pathway and plant productivity — a survey. *Zeitschrift für Pflanzenphysiologie*, 80, 1–13.

SUPPORTING INFORMATION

Additional Supporting Information may be found online in the supporting information tab for this article.

How to cite this article: Krieger C, Calvaruso C, Morlot C, Uroz S, Salsi L, Turpault M.-P. Identification, distribution, and quantification of biominerals in a deciduous forest. *Geobiology*. 2017;15:296–310.